Chapter 4

Emulsion formation via polymer brush-modified tri-compartmental microparticles

4.1 Introduction

In the previous chapter, we took brush-modified bicompartmental spherical particles [2]. This work is an extension of prior work [2]. Here, we have taken tricompartmental spherical particles. The assembly of multi-compartmental particles and their inspired designs from nature has gained global attention [204]. These particles, with anisotropic modifications, have been extensively studied for a wide range of applications such as drug delivery, Pickering emulsion stabilization, and catalysis [205,206]. Furthermore, precise surface modifications of these particles can expand the design possibilities for their assembly [7,73,206], leading to a broader range of applications. While there are diverse methods to produce multi-compartmental particles [7,73,207], very few have demonstrated precise surface modification of a specific compartment. For instance, Saha et al [110]. demonstrated the site-selective surface conjugation of a hydrophilic brush onto compositionally anisotropic microcylinders, causing differential expansion.

The controlled bending of microcylinders was caused by asymmetric expansion resulting in surface stresses. This experimental work was validated using finite element simulations to observe the bending trends. Chang and the group [208] utilized functional Polystyrene particle (PS-Br) to synthesize patchy particles through seed-mediated heterogeneous nucleation. They employed 3-(trimethoxysilyl) propyl methacrylate (TPM) or 3-(trimethoxysilyl) propyl acrylate (TMSPA) as monomers in their process. By employing controlled radical polymerization (ATRP) [51], TPM or TMSPA created polymeric patches on various functional polymeric seeds (PS-Br) formed by nucleation. ATRP [51] provided control over the morphology of compartmentalized particles and allowed for orthogonal surface modifications. Furthermore, it demonstrated the ability to reshape the particles via individual patches formed by site-selective polymerization [209]. In a recent study, Rahamani et al [111]. presented the development of innovative MPs. These included two-patch and three-patch (tri-compartmental) structures made of polylactide (PLA)/PLGA. The fabrication process involved a combination of electro-hydrodynamic co-jetting (EHDC) technique and orthogonal surface modifications. Similarly, Ifra et al [210]. revealed the spatio-selective brush grafting on cup-shaped MPs with a unique topological structure. These particles were composed of a blend of PLA and poly[methyl methacrylate-co-2-(2-bromopropionyloxy) ethyl methacrylate] (poly(MMA-co-BEMA)) in a 75/25 ratio. The study found that the brush-modified cup-shaped particles exhibited double the efficiency in adsorbing dye compared to disc-shaped particles. This discovery underscores the considerable advantage of utilizing cup-shaped particles for immobilizing and adsorbing charged species, particularly sensitive biomolecules. The researchers used brush-modified JPs to stabilize Pickering emulsion due to their amphiphilic nature [210].

Despite previous exploration of anisotropically modified particles in stabilizing Pickering emulsion, the specific architectural role of these amphiphilic colloidal surfactants in forming stable emulsion has not been thoroughly investigated. Emulsions stabilized by colloidal surfactants have distinct advantages over emulsions stabilized by conventional molecular

surfactants. Firstly, it requires significantly more energy for colloidal surfactants to detach from the water/oil interface, leading to permanent attachment and exceptional stability [211]. Secondly, colloidal surfactants can be composed of biocompatible substances, thus exhibiting excellent biocompatibility [212]. Lastly, colloidal surfactants can be engineered to create Pickering emulsions with various functionalities, such as pH, temperature, or light-induced reactions [213].

In various literature reports, including our own [2,40,124], it has been shown that JPs with a perfect balance of amphiphilicity are excellent at stabilizing Pickering emulsions. Building on the success of our previous study, we decided to synthesize multi-compartmental particles instead of bi-compartmental ones, and selectively modify them to have both chemical and structural anisotropy. This approach may expand the scope and application areas of these particles. In this specific study, we attempted to create tri-compartmental particles using the EHDC technique, and then allowed poly(DMAEMA) as well as poly(EGMA) brushes to grow from one or two of the tri-compartments. This method yields a wide range of anisotropic particles with varying amphiphilicity, which can be studied for their architectural influence in stabilizing Pickering emulsions beyond Janus geometry. We conducted simulation studies to gain a better understanding of the microscopic processes that occur in our system. These studies complement our experimental results on oil-in-water emulsion via polymer brush-modified tri-compartmental Janus particles (TPs). To perform the simulations, we utilized the DPD simulation technique [22], which involves coarse-graining the system into interacting beads treated as point particles. The system dynamics are tracked using Newton's equation of motion [22,23,35,37]. DPD simulation offers significant advantages over traditional MD models, as it can simulate systems with greater length and time scales [22,23,35,37]. This simulation technique effectively captures the hydrodynamic behavior of polymer chains in various states, including solution [144], melt [145], and biopolymers [1]. Thus, it can realistically imitate the polymeric system's static and dynamic features. However, when applying DPD [149,150,214]

to model biological systems, the incorporation of charge distribution and direct inclusion of electrostatic forces is rarely addressed [151]. We modeled the polymer brushes as a linear chain of soft particles (beads) connected by harmonic bonds [152].

In the experiment, we grew poly(DMAEMA) brushes by introducing poly(MMA-co-BEMA) initiators onto the tri-compartmental MP surfaces. We initiated the surface-initiated ATRP of DMAEMA monomers in an aqueous medium to start this reaction [1,145]. In our experiment, we studied the oil-in-water emulsion using polymer brush-modified tri-compartmental particles (TPs) at $pH = 7$. The poly(DMAEMA) brushes and MP surfaces were positively charged within the solvent at $pH = 7$ [40,73,123]. Due to the electrostatic repulsion, the brushes and MPs efficiently scattered throughout the solvent, preventing them from aggregating. We established an excellent correlation between the experimental and simulation results. Here, I wil; discuss only the

4.2 Simulation methodology

4.2.1 DPD simulation

The DPD [22,28] method is a widely used computational tool for studying free radical polymerization [35] processes and exploring the dynamic characteristics of soft materials [1]. In this study, we created rigid spherical MPs using 90% PLA and 10% poly(MMA-co-BEMA). The poly(MMA-co-BEMA) serves as an initiator for the ATRP [7,40,123,124] of DMAEMA monomers in the solution [172,180,185], which leads to the formation of polymer brushes on the surface of the MPs. In addition to serving as initiators, the MPs are hydrophobic due to the 90% PLA composition. Our goal is to investigate the impact of this approach on oil-in-water emulsion using polymer brush-modified TPs. Previous research provides detailed information on the ATRP technique and the parameters used to modify MPs through the DPD simulation technique [1,2]. Our ATRP-brush modification involves initiating and propagating DMAEMA

monomers, following the established procedure from prior DPD simulations [1,2]. All the system components, including initiators and monomers, are represented by DPD beads. The LAMMPS software integrates the equations of motion for DPD simulations [215]. Here the polymerization process, cut off radius, initiation probability, propagation probability, bond potential, equilibrium bond length, angle potential, equilibrium angle and other parameters are same as previous chapter [2].

We will start the simulation with $50r_c \times 50r_c \times 50r_c$ (in reduced DPD units) simulation box, which is equal to a box size of $48.5nm \times 48.5nm \times 48.5nm$ in actual units. The simulation box contains a total of 3.75×10^5 DPD beads. We maintain an overall number density of $\rho = 3$ [22,23] within the box. The periodic boundary condition is enforced in all directions.

4.2.2 Constituting microparticle

We modeled the MPs as three layers of DPD beads arranged on a geodesic grid [48]. Each layer contains a fixed number of DPD beads. The inner and outer radii are defined as $R_{in} = 1.2r_c$ and $R_0 = 2.0r_c$ for a system with $N_{MP} = 30$ MPs. This results in $n_{MP} = 1086$ DPD beads per MP and a total of 32580 MP beads in the system, with a volume fraction of $\phi_{MP} = 8.6 \times 10^{-2}$. We treated the MP as a rigid body and calculated the combined force and torque acting on it by summing the forces and torques exerted on its constituent DPD beads [22]. Furthermore, we maintained a high bead density ($\rho_m \gg 3$) in each layer to prevent ATRP-brush or other beads from entering the MP [1,2,124].

In the experimental studies, the poly (BEMA) molecules, which are embedded on one-third $(1/3)$ or two-thirds $(2/3)$ of the outer surface of the MPs, serve as initiators in the system. To simulate this, we randomly select a specific number of DPD beads on the top surface of $1/3$ and $2/3$ of the MPs to act as initiators for the ATRP process in the solution [22,28]. We analyzed the data using an initiator concentration of approximately 3% n_{MP} on $1/3$ of the MP's outer surface and approximately 6% n_{MP} on $2/3$ of the MP's outer surface for each type of MPs.

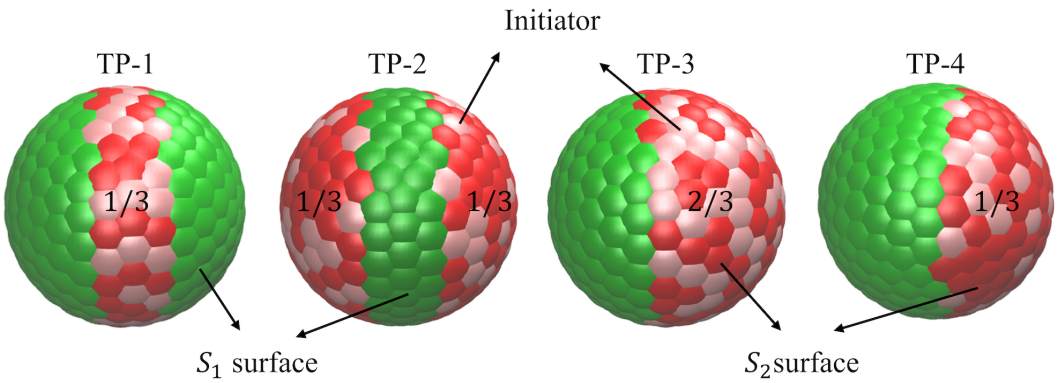

Fig. 4.1: Figure shows the TP-1, TP-2, TP-3, and TP-4 type MPs.

The corresponding types of MPs are named TP-1, TP-4 and TP-2, TP-3, respectively. The initiator volume fraction for $1/3$ and $2/3$ of the surfaces are $\phi_i = 2.64 \times 10^{-3}$ and 5.28×10^{-3}, respectively.

Initially, we randomly placed initiator-embedded 30 MPs in the simulation box and then introduced the initial configuration of DMAEMA monomer and solvent beads in the simulation box. The volume fraction of monomer and solvent beads are $\phi_M = 2.5 \times 10^{-1}$ and $\phi_S = 6.1 \times 10^{-1}$, respectively. The system was then equilibrated for $t = 5.0 \times 10^4 \Delta t = 1000\tau$ to ensure that the initial configuration of the moieties and solution has no apparent impact on the diffusion between the MPs and the solution. After the equilibration phase, the ATRP reactions to grow the polymer brushes on the MP's surface were initiated. Subsequently, oil beads were introduced into the system. The oil beads are modeled similarly to the solvent. The volume fraction of oil particles in the system is $\phi_o = 0.5 \times 10^{-1}$. The whole system was again equilibrated at high temperature $T = 5$, and then the temporal evolution of oil and water was monitored at temperature $T = 1$ for emulsification time up to $t = 1.2 \times 10^4 \tau$.

To ensure that beads of similar types are compatible, the DPD repulsive interaction parameter is typically set at $a_{ii} = 25$ [22,28]. The maximum repulsive interaction parameter ($a_{ij} = 60$) [22,28] for oil beads is set because they are not compatible with brushes and water beads. However, oil and MPs' hydrophobic surface can coexist chemically (compatible with each other), we set $a_{ij} = 25$. On the other hand, the poly (DMEAMA) brushes have an interaction

parameter with water of $a_{ij} = 25$, as they are compatible with water beads. See Table 4.1 for a comprehensive list of all the interaction parameters used.

Table 4.1: The interaction parameter a_{ij} used in the simulation for different DPD beads.

a_{ij}	S	MP	i	M	B	O
$Solvent(S)$	25	60	30	25	27	60
$Microparticle(MP)$		30	30	40	40	25
$Initiator(i)$			30	30	30	45
$Monomer(M)$				25	25	60
$Brush(B)$					27	60
$Oil(O)$						25

4.2.3 Brush-modification of microparticles

The description of brush modification surfaces via ATRP process is given in section 1.7 and also given in previous chapter. We modified the MPs by introducing the initiators on the outer surface of MPs and polymerize them at different time.

4.2.4 Characterization function for morphology and the characteristic length scale

We use the two-point equal-time correlation function. The detail of these characterization function and characteristic length scale are given in previous chapter's section 3.2.4.

In our simulation, we have observed that as $C(r,t)$ decays to 0.2, it provides an accurate estimate of $R(t)$. However, other definitions within the scaling regime also yield comparable values of $R(t)$, differing only by constant multiplicative factors. The average domain size typically follows a power-law curve: $R(t) \rightarrow at^{\phi}$, where "$a$" is a constant and ϕ represents the growth exponent [29]. It is important to note that DPD simulations are known for accurately representing the hydrodynamic behavior of multicomponent fluid mixtures. Therefore, the

period of diffusive growth ($\phi \sim 1/3$) is short-lived for any typical phase separating binary fluid. The system quickly transitions to hydrodynamic regimes: initially $\phi \sim 1$ (viscous hydrodynamic), and later to another crossover at $\phi \sim 2/3$ (inertial hydrodynamic) [29,216].

4.3 Results and discussion

We initiate the growth of polymer brushes by starting with monomers in solution and using the ATRP method via the DPD simulation. This process begins by initiating them from randomly distributed initiators on designated outer surfaces of MPs. To analyze the kinetics of the polymer reaction, we plot the time variations of monomer conversion. Monomer conversion is calculated as $Conv_M = [M]_r/[M]_0$, and $\log([M]_0/[M]_u)$ is plotted in Fig. 4.2(a) and Fig. 4.2(b), respectively, up to a brush-growth time $t_{bg} = 8 \times 10^2$. Here, $[M]_0$ represents the initial monomer concentration, while $[M]_r$ and $[M]_u$ indicate the concentrations of reacted and unreacted monomers at time t_{bg}. We have taken initiator concentration $c_i \simeq 3\%$ of n_{MP} for TP-1 and TP-4 type MPs, and $c_i \simeq 6\%$ of n_{MP} for TP-2 and TP-3 type MPs. Here, $n_{MP} = 1086$ denotes the number of DPD beads per MP. From the red and green curves, we observe that TP-2 and TP-3 MPs exhibit higher monomer conversion (23.2% and 26.6% of N_M) and faster polymer growth rates compared to TP-1 and TP-4 (13.7% and 14.7% of N_M), denoted by the black and blue curves. Here, $N_M = 93750$ represents the number of initial monomer beads in the system. This difference occurs because the former MPs have double the initiator concentration, which leads to more efficient ATRP brush growth. Importantly, initiators are more easily reached by monomers at the outer region of spherical MPs (as in TP-4) compared to the central region (as in TP-1). This explains the lower monomer conversion and rate kinetics observed in TP-1 and TP-3 type MPs compared to the corresponding TP-2 and TP-4 type MPs based on the number of initiators. It is important to note that these illustrated curves only depict initial monomer conversion.

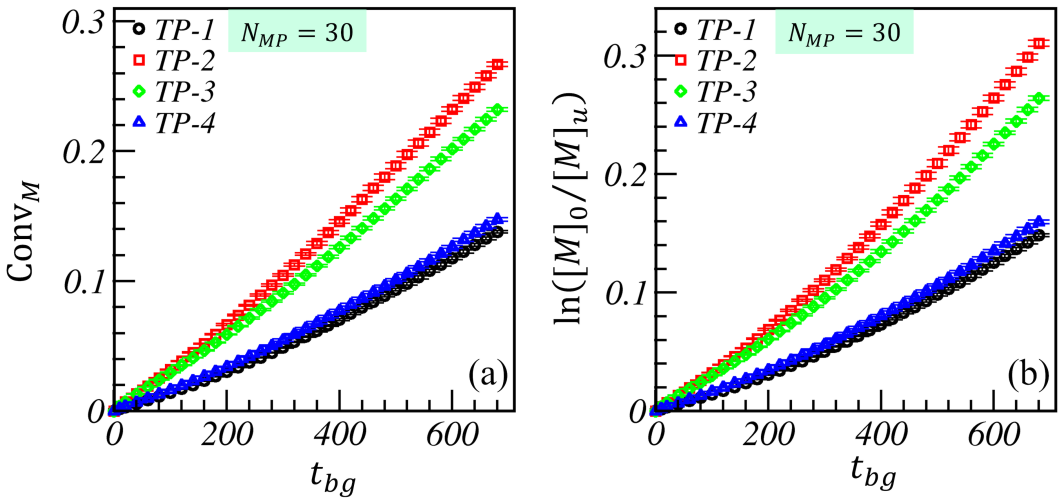

Fig. 4.2: (a) The graph shows the monomer conversion ($Conv_M$ vs. t_{bg}) during the growth of polymer brushes with different initiator concentrations. For TP-1 and TP-4 MPs, the initiator concentration (c_i) is about 3% of (n_{MP}), while for TP-2 and TP-3 MPs, the initiator concentration is about 6% of n_{MP}. The curves on the graph represent the monomer conversion for four types of MPs: TP-1 (black), TP-2 (red), TP-3 (green), and TP-4 (blue). The initiators are embedded on the outer surface of the MPs, and the study involves a total of 30 MPs.

We observe $Conv_M$ approaching 1.0 at much later times, as shown in Fig. 4.3(a) for TP-1 (black curve), TP-2 (red curve), TP-3 (green), and TP-4 (blue). Fig. 4.2(b) demonstrates linear polymerization kinetics at early times: $\ln([M]_0/[M]_u)$ vs. t_{bg} for similar. Additionally, the reaction rate kinetics deviate slightly from linearity at late times when $Conv_M$ approaches 1.0 in Fig. 4.2(b), indicating pseudo-first-order kinetics. Thus, our model successfully captures the expected characteristics of living radical polymerization rate kinetics, resulting in polymer brush-modified TPs [36,37,71].

To investigate the impact of different brush-modified TPs in stabilizing emulsion, we varied the ATRP brush growth time to produce fabricated TPs denoted as TP-1 to TP-4, with each TP possessing an average brush length (degree of polymerization) $l_b \simeq 7$. At the start of the emulsification process, the volume fractions of oil and solvent are set as $\phi_o = 5.0 \times 10^{-2}$ and $\phi_s \simeq 8.3 \times 10^{-1}$, respectively. We observed the emulsification of oil for $t = 1.2 \times 10^4$, as shown in Figs. 4.4(a-d) for the four types of MPs. In the figures, polymer brushes are blue, oil beads are yellow, and the green and red beads represent the hydrophobic surfaces of the MPs. We

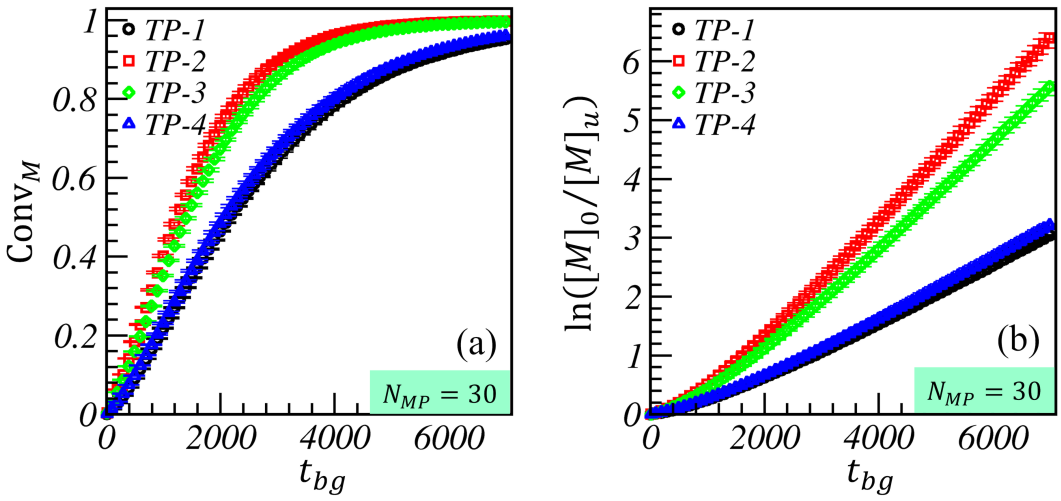

Fig. 4.3: Comparison of the temporal variation of monomer conversion ($Conv_M$) in (a) and $\ln([M]_0/[M]_u)$ in (b) for TP-1 (black), TP-2 (red), TP-3 (green), and TP-4 (blue) MPs. In (a), the monomer conversion demonstrates a linear behavior at early times and converges towards one at later times for all cases. In (b), there is a linear relationship between natural logarithm of $([M]_0/[M]_u)$ and time. The green and red curves show a slight deviation from linearity when $Conv_M \rightarrow 1.0$ at much later times.

used different colors and labels to distinguish between the initiator (pink) embedded surface (S_2) and the non-embedded surface (S_1).

To enhance visual clarity, water beads as a solvent have been excluded from the images. Figs. 4.4(a-d) clearly show the formation of emulsions for TP-1, TP-2, TP-3, and TP-4 MPs. On the other hand, TP-2 MPs exhibits highly unstable oil-in-water emulsification due to its specific topology. The central region (S_1 surface) of the TP-2 is compatible with oil, but the hydrophilic polymer brushes on the remaining regions (S_2 surface) hinder the movement of oil beads to the S_1 surface. As a result, we observed the formation of a large oil phase nucleus, which is a characteristic of off-critical immiscible binary fluid phase separation [9,10,12].

In order to analyze the emulsion morphology, we start by examining the radial distribution function (RDF), which is denoted as $g(r) = \rho_l/\rho_T$, in Fig. 4.4(e) for oil beads surrounding the S_1 (hydrophobic) surface beads of MP. This corresponds to the oil-in-water emulsion shown in Figs. 4.4(a-d). Here, ρ_l represents the local oil density around a reference red bead on the S_1 surface within a shell of width $dr = \sqrt{|x|^2 + |y|^2 + |z|^2}$, and ρ_T is the total oil density in the

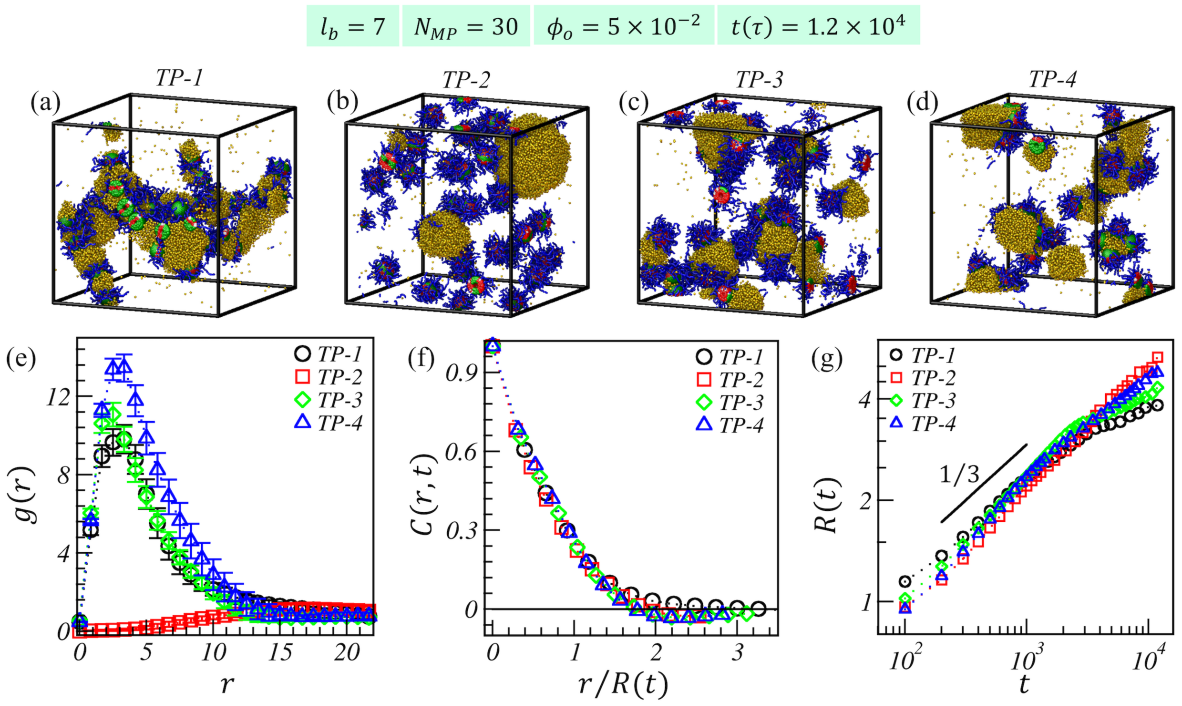

Fig. 4.4: The images (a-d) illustrate the oil-in-water emulsion morphology using polymer brush-modified four types of MPs: TP-1, TP-2, TP-3, and TP-4. The length of the polymer brush is constant at $l_b \simeq 7$, and the emulsification time is set at $t = 1.2 \times 10^4$. Solvent (water) beads are omitted for clarity. In (e-g), the radial distribution function (RDF) $g(r)$ vs. r, the scaled correlation function $C(r,t)$ vs. $r/R(t)$, and the characteristic length scale $R(t)$ vs. t are presented at the emulsification time, $t = 1.2 \times 10^4$ for brush modified TP-1, TP-2, TP-3, and TP-4. The oil concentration in the system is set at $\phi_0 = 5.0 \times 10^{-2}$.

system. Due to topological constraints, the S_1 surface comprised of $2/3$ of TP-1 and TP-4 MPs. However, in TP-4, the entire S_1 surface is located on one side, while in TP-1, the S_1 surface is evenly separated by the brush-modified S_2 surface (making up $1/3$ of the MP) in the middle. As a result, oil beads find the S_1 surface of TP-4 more easily accessible than TP-1, leading to a higher RDF peak and width, as indicated by the blue symbols compared to the black curve for TP-1. On the other hand, for TP-2 MPs, the S_1 surface is situated between brush-modified hydrophilic S_2 surfaces, making it significantly more challenging for oil beads to access. This explains the reduced RDF peak (red curve) observed for TP-2 MPs.

The emulsion morphologies were further analyzed using the scaled correlation function, $C(r,t)$ vs. $r/R(t)$, shown in Fig. 4.3(f) at $t = 1.2 \times 10^4$. The green and blue scaling function

data for TP-3 and TP-4 type MPs revealed significant overlap, indicating statistical similarity in the emulsion morphologies. This similarity is due to their comparable topology, with S_1 and S_2 surfaces on opposite sides of the MPs. It is important to note that the topology of TP-1 and TP-2 type MPs differs from each other and also from TP-3 and TP-4 type MPs. As a result, there is a clear departure from dynamic scaling in the scaled correlation function data for TP-1 (black curve) and TP-2 (red curve) compared to their corresponding TP-3 and TP-4 data.

For the emulsion formation, the characteristic growth law, $R(t)$ vs. t, is shown in Fig. 4.4(g) for up to $t = 1.2 \times 10^4$ [9,10,12]. It is important to note that the oil-in-water system used for emulsion formation can be considered a highly off-critical binary mixture. As a result, the characteristic length scale follows the typical diffusive growth ($\phi \sim 1/3$) during the initial stages when the oil nucleus develops within the water phase. During this short period, brush-modified TPs diffuse to the oil-solvent interface. The interface wetting by TPs reduces interfacial tension, which in turn limits the growth of oil clusters. The length scale gradually transitions to a saturation regime instead of moving into the hydrodynamic regimes, confirming the stabilizing effect of oil emulsification in water. Our results strongly indicate that the length scale tends to saturate much earlier, resulting in a smaller average domain size in the presence of TP-1 (black curve), followed by TP-3 (green curve), and TP-4 (blue curve), indicating the order of stable emulsification. However, for TP-2 (red curve), the length scale continues to grow, resembling the typical phase separation behavior of off-critical binary fluid mixtures. This implies a much less stable emulsion formation, as expected from the morphology image in Fig. 4.3(b) and the corresponding RDF plot (red curve) in Fig. 4.3(e). Nevertheless, we note a much larger domain size than the other three cases, which continues to grow at late times and is saturated at late times due to the finite size effect where cluster size becomes equivalent to the system size, and there is no further kinetics in the system [9,10]. This confirms that stable emulsification does not occur for TP-2. Thus, the stabilizing trend obtained for the emulsion formation in our system is as follows: TP-1 > TP-3 > TP-4 > TP-2. In our experiments, we

observed that the emulsion stability order was slightly different from what we had originally stated. TP-1 showed the least stability, while the stability order for the other TBPs remained the same: TP-3 > TP-4 > TP-2. This difference could be attributed to the positioning of the macroinitiators, resulting in the formation of a dense brush layer at the center of TP-1 MPs with a high brush density. This dense and hydrophilic polymer brush matrix may have hindered the diffusion of oil droplets, leading to the creation of a stable network-like emulsion of oil-in-water. However, TP-1 MPs failed to provide such stability at low to moderate grafting density, as observed in both experiments and simulations.

In Fig. 4.5, we demonstrate how varying brush lengths affect the emulsification of oil ($\phi_o = 5.0 \times 10^{-2}$) in the solvent ($\phi_s \simeq 8.3 \times 10^{-1}$). The parameters, including the number of monomer ($N_{MP} = 30$), initiators ($c_i \simeq 3\%$ and 6% of N_{MP}), and monomer volume fraction ($\phi_M = 2.5 \times 10^{-1}$), remain consistent with previous cases. Polymer brushes were allowed to grow on the initiator-embedded fraction of TPs at different times to achieve 2 different average brush lengths, such as $l_b \simeq 7$ and 14 (in reduced DPD units) for all four types of TPs.

Fig. 4.5(a) compares the characteristic cluster size of emulsion, $R(t)$ vs. t, on a log-log scale for TP-1 and TP-4 type MPs, where one-third of the TP's fraction is polymer brush-modified. The black and red curves represent $R(t)$ for $l_b \simeq 7$, while the green and blue curves represent $l_b \simeq 14$. In Fig. 4.5(b), a comparison is made between TP-2 and TP-3 MPs, where two-thirds of the TP's fraction is polymer brush-modified, for $l_b \simeq 7$ and $l_b \simeq 14$. The solid black line represents the early-time diffusive growth exponent $\phi \sim 1/3$. Both plots indicate that as the brush length increases, $R(t)$ saturates earlier, resulting in smaller and stabilizing emulsion formation for each type of TP, with nominal emulsion for TP-2 type particle.

In another scenerio, we grew the polymer brushes on S_2 surfaces while keeping the total monomer conversion in the system constant. To achieve a monomer conversion of approximately $14.7\% N_M(Conv_M)$, we are using the ATRP process with different brush growth times: $t_{bg} = 720$, 400, 460, and 680 for TP-1 to TP-4 type MPs. TP-1 and TP-4 have half the number

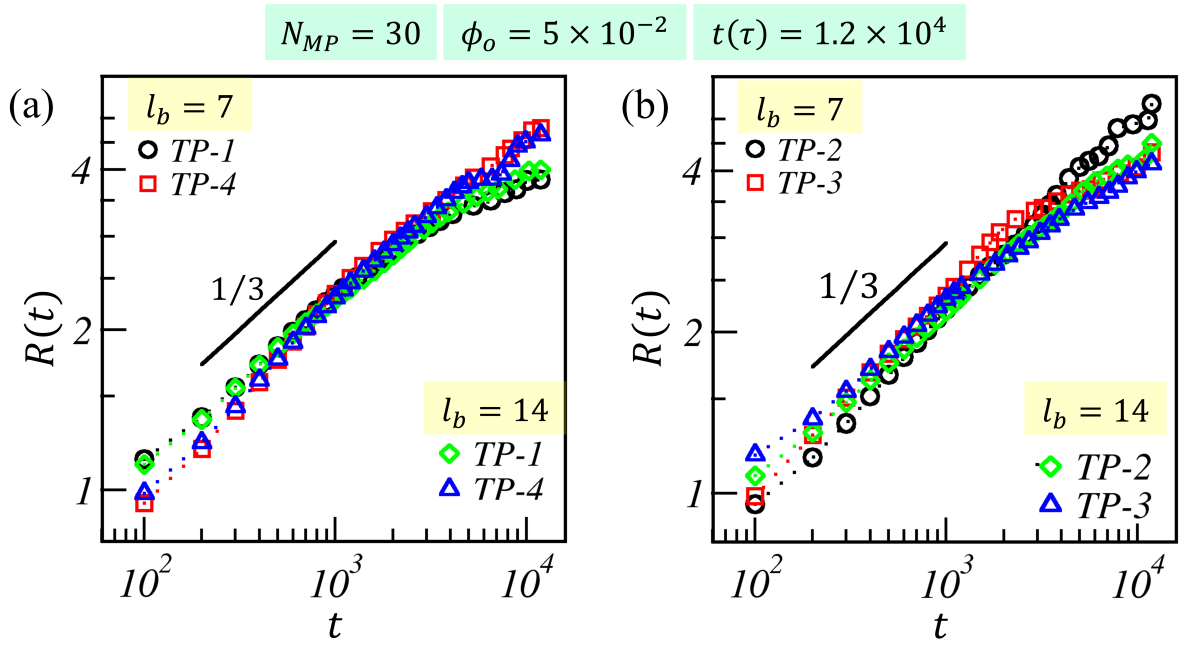

Fig. 4.5: Comparison in the length scales ($R(t)$ vs. t) for the oil-in-water emulsion morphology of (a) TP-1 and TP-4 type MPs and (b) TP-2 and TP-3 type MPs at $l_b \simeq 7$ and $l_b \simeq 14$, respectively. The emulsification time is set at $t = 1.2 \times 10^4$ and $\phi_0 = 5.0 \times 10^{-2}$.

of initiators compared to TP-2 and TP-3, resulting in approximately double the brush length for TP-1 and TP-4 ($l_b \simeq 14$) compared to TP-2 and TP-3 ($l_b \simeq 7$). However, the overall brush density in the system remains the same.

In Fig. 4.6(a), the radial distribution function (RDF) for oil beads around the S_1 surface shows that TP-2 has a lower peak than the other modified TPs due to topological constraints. The S_1 surfaces were constrained mainly on the sides of TP-1, TP-3, and TP-4 MPs, making them more accessible to oil beads than TP-2 MPs. The corresponding RDFs for TP-1, TP-3, and TP-4 display higher peak strengths, represented by the black, green, and blue curves in Fig. 4.6(a). TP-4 has a high peak strength and width due to its larger S_1 surface area on one side of the MPs. Additionally, in Fig. 4.6(b), the average domain size ($R(t)$ vs. t) is plotted up to emulsification time $t = 1.2 \times 10^4$, revealing diffusive growth ($\phi \sim 1/3$) for all data sets at initial times. As time progresses, the cluster growth rate slows down, indicating the formation of stable emulsions. The black curve representing TP-1 emulsion is the most stable, followed

by the green curve representing TP-3, and the blue curve representing TP-4, while the red curve representing TP-2 shows negligible emulsion formation.

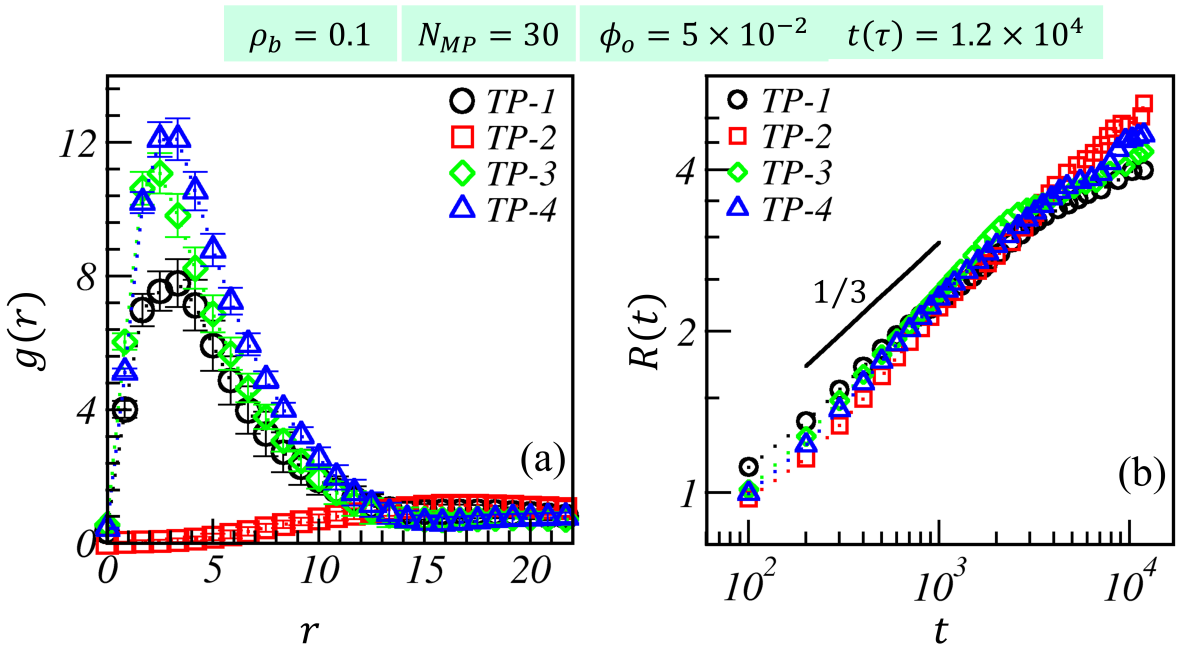

Fig. 4.6: (a) Comparison of RDF ($g(r)$ vs. r) for the emulsification time $t = 1.2 \times 10^4$ for oil beads around S_1 surface at a constant brush density, where overall monomer conversion in the system is kept constant for all TPs. (b) Shows the characteristic length scale ($R(t)$ vs. t) on a log-log scale for TP-1, TP-2, TP-3, and TP-4 MPs denoted by black, red, green, and blue symbols, respectively.

We investigated how different brush densities of TPs affect oil emulsification. In Fig. 4.7(a-c), we show the oil emulsification of TP-1 MPs with three different brush densities ($\rho_b \simeq 0.01, 0.02$, and 0.05) and the same brush length ($l_b \simeq 7$) at the emulsification time, $t = 1.2 \times 10^4$. To modify the TPs with different brush densities while keeping the same brush length, we used three different initiator concentrations ($c_i = 0.6\%, 1.3\%$, and 3.0% of n_{MP}) on the TP-1 MP surface. We then allowed the ATRP to occur at different brush growth times. We followed the same process for TP-3 and TP-4 MPs, which we will explain shortly.

In Fig. 4.7(c), we observe a change in the emulsion morphology at high brush density compared to the structures in Figs. 4.7(a) and 4.7(b) at lower densities. This suggests that TP-1 MPs create a more stable emulsion at higher brush density. To gain a deeper understanding of

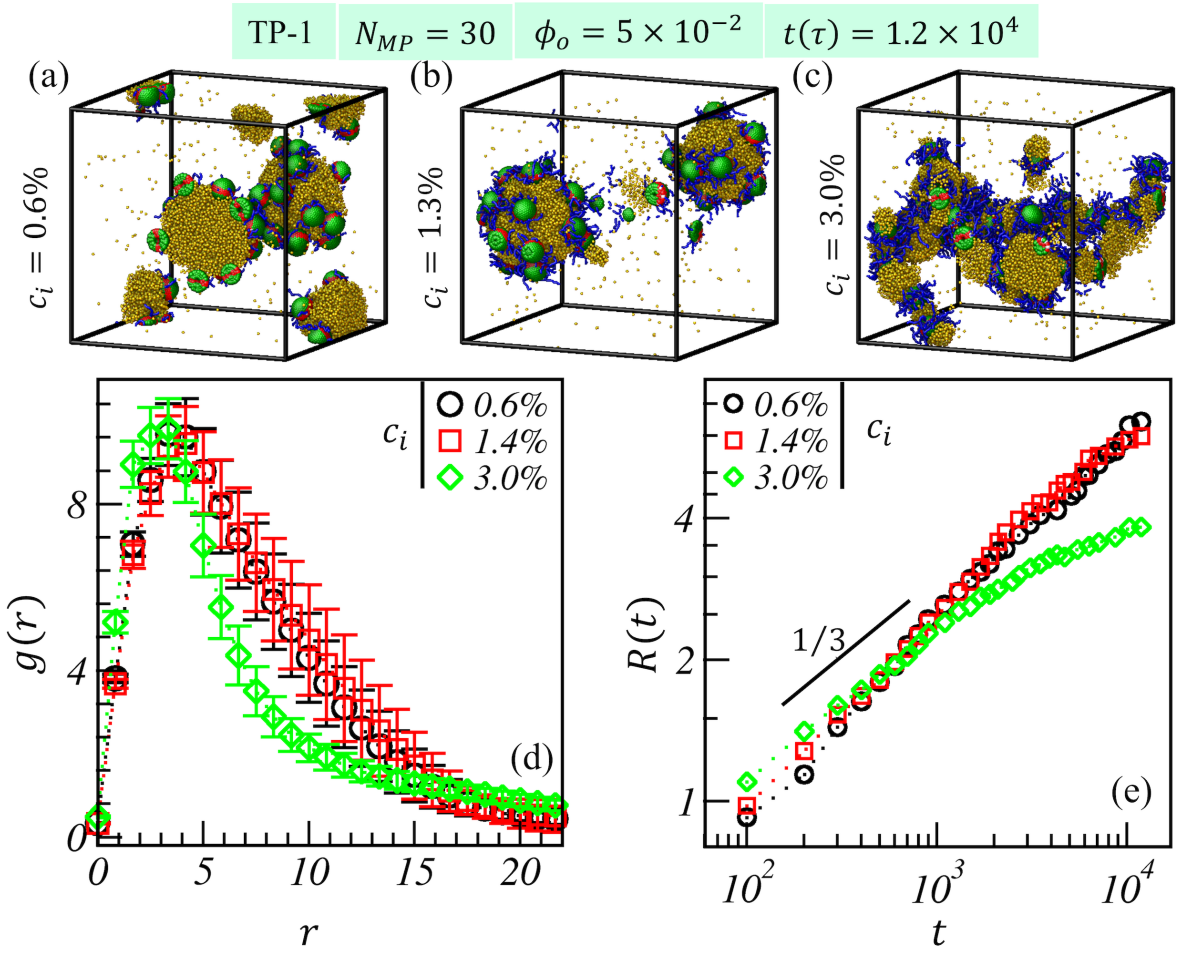

Fig. 4.7: The graphs (a-c) illustrate the evolution of oil emulsion morphology using polymer brush-modified TP-1 MPs at different brush densities (ρ_b) of approximately 0.01, 0.02, and 0.05, while maintaining a constant brush length (l_b) of approximately 7 for an emulsification time of $t = 1.2 \times 10^4$. Graph (d) compares the radial distribution function (RDF) ($g(r)$ vs. r) for oil beads around the S_1 surface. (e) shows the time variation of length scale ($R(t)$ vs. t) at different brush densities for TP-1 MPs.

emulsion morphologies depicted in Fig. 4.7(a-c), we present the RDF for oil beads surrounding the hydrophobic (S_1) surfaces of MPs (TPs) in Fig. 4.7(d). The wider RDF indicates that the oil droplets are more spread out around the TPs when they can easily move through the S_2 surface with fewer brush beads (black and red curves). However, when the brush density is high (as seen with the green curve), the oil transport across the surface is inhibited, resulting in a narrower RDF width around the MPs. The length scale curves are plotted for emulsification time up

to $t = 1.2 \times 10^4$. The green curve in Fig. 4.7(e) represents the corresponding characteristic length scale ($R(t)$ vs. t), which tends to saturate much earlier, resulting in a stable and reduced average domain size. At the S_2 surface of TP-1 MPs, the lower brush density creates a more porous brush-water interface. The oil beads around the S_1 surfaces of MPs can diffuse through the interface and form a larger oil phase nucleus due to typical phase separation kinetics for an off-critical immiscible binary fluid. In Fig. 4.7(e), the black and red curves show the related characteristic length scale, demonstrating a slight slowdown at late times, indicating less stable emulsion formation, and then reaching saturation, confirming the system's finite size effect. However, as the brush density increases, the porosity of the brush-water interface decreases, which minimizes the oil diffusion through the interface. Therefore, density plays a key role in creating a stable oil-in-water emulsion for TP-1 MPs.

Further, we studied the effect of different brush densities on emulsification using TP-3 and TP-4 type MPs. We ensured that the brush length ($l_b \simeq 7$) remained consistent by modifying the initiator-embedded S_2 surfaces of MP at different times for varying initiator concentrations. For TP-3 type MPs, with $c_i = 1.3\%$, 3.0%, and 6.0% of n_{MP} was kept at the brush growth time $t_{bg} = 2.9 \times 10^2, 3.3 \times 10^2$, and 4.6×10^2, respectively. The corresponding brush densities were $\rho_b \simeq 0.02, 0.05$, and 0.11. Similarly, for TP-4 MPs, $t_{bg} = 2.9 \times 10^2, 3.3 \times 10^2$, and 3.9×10^2 for $c_i = 0.6\%, 1.4\%$, and 3.0% of n_{MP}, respectively, with brush densities $\rho_b \simeq 0.01, 0.02$, and 0.05.

Figs. 4.8(a-c) and 4.8(d-f) depict the of oil-in-water emulsions morphologies for TP-3 and TP-4 type MPs, respectively, with varying brush densities. These images demonstrate that higher brush density leads to increased stability in emulsion formation. Furthermore, Fig. 4.8(g) for TP-3 and Fig. 4.8(h) for TP-4 show the average domain size $R(t)$ vs. t for time up to $t = 1.2 \times 10^4$, indicating typical diffusive growth ($\phi \sim 1/3$) for all datasets at initial times. As time progresses, the rate of cluster growth slows down, suggesting the formation of more stable emulsions with higher brush density, as indicated by the green curves. We omitted the results

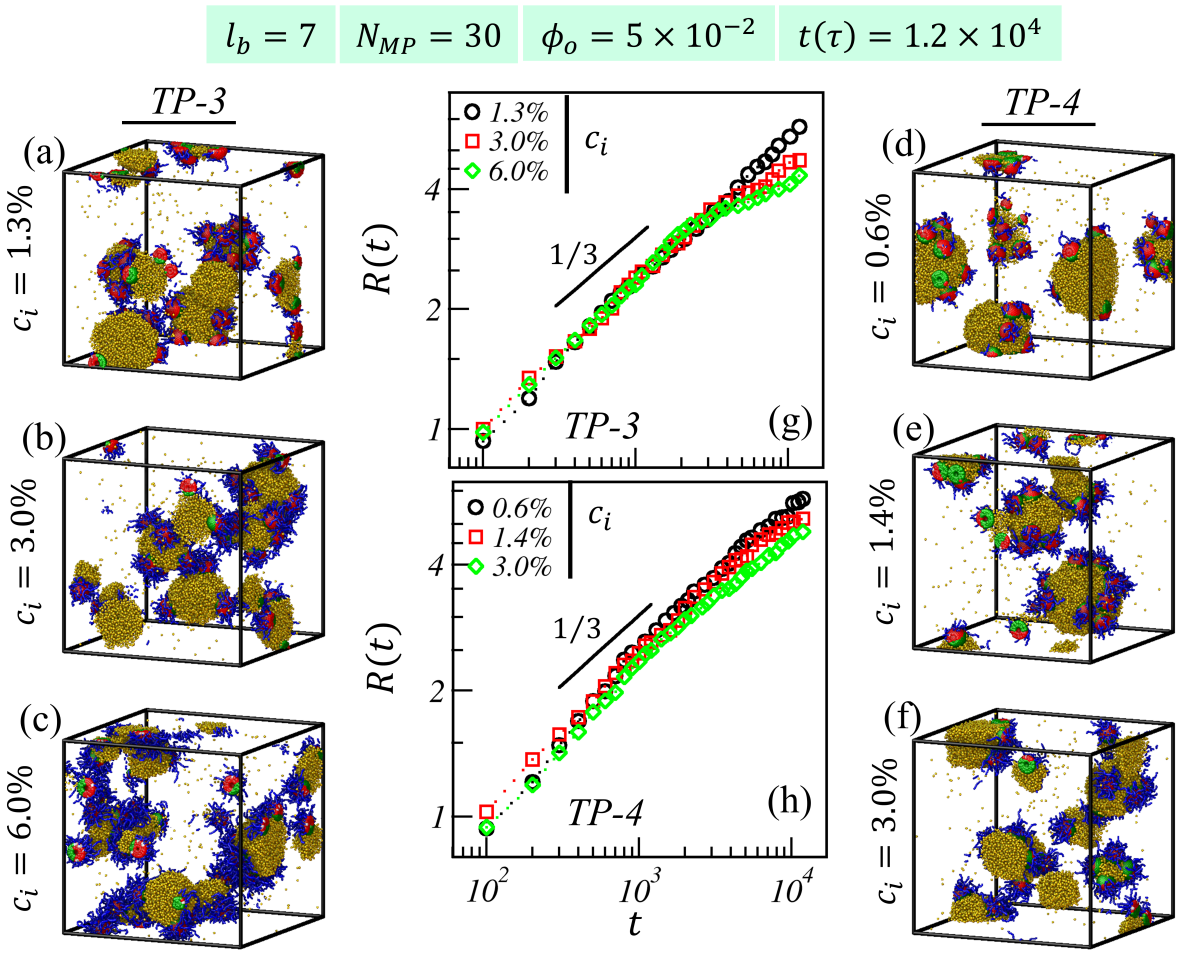

Fig. 4.8: (a-c) Morphologies of oil emulsion for different brush densities, $\rho_b \simeq 0.02$, 0.05, and 0.11 for TP-3 at $t = 1.2 \times 10^4$. (d-f) Morphologies for TP-4 with $\rho_b \simeq 0.01$, 0.02, and 0.05 at $t = 1.2 \times 10^4$. The brush length, $l_b \simeq 7$, was kept constant for all the cases. Comparison of the time variation of length scale ($R(t)$ vs. t) is displayed at different brush densities for TP-3 in (g) and TP-4 in (h) for the emulsification time up to $t = 1.2 \times 10^4$.

for TP-2, as it yields the least stable oil-in-water emulsification. In addition, we analyzed the temporal variation of length scale ($R(t)$ vs. t) for all TPs at three different brush densities fig. 4.9 in while keeping the brush length fixed ($l_b \sim 7$). Our simulation results indicated that at low to moderate brush densities, the length scales for different TPs showed the order of stability as TP-3 > TP-4 > TP-2 > TP-1, which is akin to the experimental results.

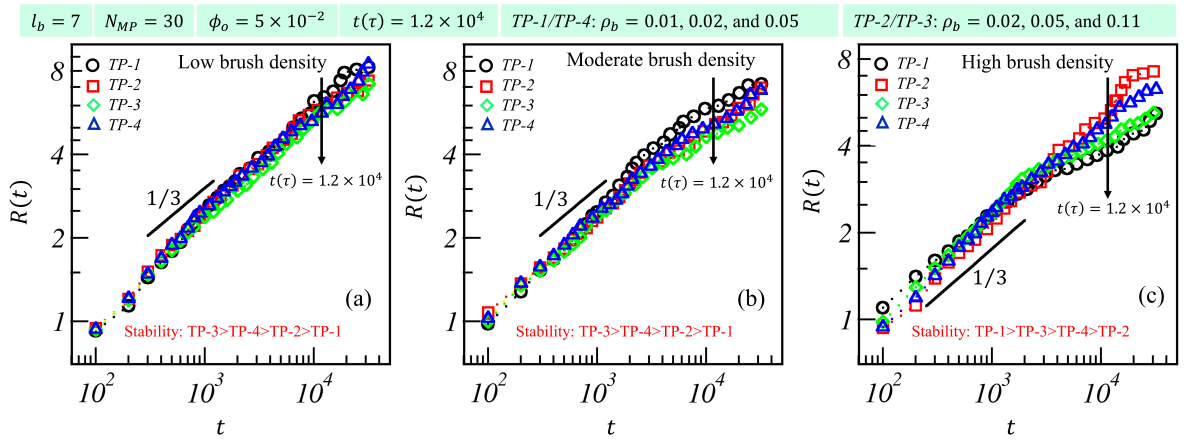

Fig. 4.9: Comparison of the length scales ($R(t)$ vs. t) for the oil-in-water emulsion for TP-1 to TP-4 MPs for (a) lower, (b) moderate, and (c) high brush density at $l_b \sim 7$. For TP-1 and TP-4, the brush density varies as $\rho_b \simeq 0.01$, 0.02, and 0.05, and for TP-2 and TP-3, the brush density varies as $\rho_b \simeq 0.02$, 0.05, and 0.11.

4.4 Conclusion

Our research involved a study using both numerical and experimental methods to create stable Pickering emulsions using ATRP brush-modified Tri-compartmental MPs (TPs). We used the DPD technique to develop a simulation model for designing brush-modified TPs through surface-initiated ATRP brush grafting on either 1/3 (TP-1 and TP-4) or 2/3 (TP-2 and TP-3) fraction of MP. The simulation results provide a detailed comparative analysis at the microscopic level. Our simulation model demonstrated linear polymer growth through reaction rate kinetics, accurately capturing the expected first-order chemical kinetics of living free radical polymerization.

In our observations, we found that using TP-1 significantly increased the stability of oil-in-water emulsion on different TPs, with TP-3 and TP-4 close behind. TP-2 type MPs showed very little stability. When we varied the polymer brush length on the same type of MPs, we noticed that longer brushes resulted in a more stable emulsion. The consistent monomer conversion in the system indicates a uniform brush density while changing the brush length. The decrease in c_i was associated with longer brush lengths, leading to improved interface wetting and

increased stability of the oil-in-water emulsion. The order of emulsion stability was as follows: TP-1 > TP-4 (lower c_i) and TP-3 > TP-2 (higher c_i). Additionally, we found that increasing the brush densities for TP-1, TP-3, and TP-4 also led to more stable emulsion formation. Overall, our simulation results align with the experimental findings.